



HAL
open science

Flexible barrier and flow-driven woody debris: an experimental investigation of their interaction

Stéphane Lambert, Firmin Fontaine, Guillaume Piton

► To cite this version:

Stéphane Lambert, Firmin Fontaine, Guillaume Piton. Flexible barrier and flow-driven woody debris: an experimental investigation of their interaction. *European Journal of Environmental and Civil Engineering*, 2023, pp.1-23. 10.1080/19648189.2023.2268706 . hal-04250117

HAL Id: hal-04250117

<https://hal.science/hal-04250117>

Submitted on 20 Oct 2023

HAL is a multi-disciplinary open access archive for the deposit and dissemination of scientific research documents, whether they are published or not. The documents may come from teaching and research institutions in France or abroad, or from public or private research centers.

L'archive ouverte pluridisciplinaire **HAL**, est destinée au dépôt et à la diffusion de documents scientifiques de niveau recherche, publiés ou non, émanant des établissements d'enseignement et de recherche français ou étrangers, des laboratoires publics ou privés.

Flexible barrier and flow-driven woody debris: an experimental investigation of their interaction

5 Stéphane Lambert¹, Firmin Fontaine¹, Guillaume Piton¹

¹Univ. Grenoble Alpes, INRAE, CNRS, IRD, Grenoble INP, IGE, 38000 Grenoble, France

Correspondence to: Stéphane Lambert (stephane.lambert@inrae.fr)

DOI: 10.1080/19648189.2023.2268706

10

Abstract

Flexible barriers have been recently proposed as a promising alternative for trapping woody debris driven by the flow in torrents and rivers before they reach elements at risks. Small-scale experiments in similitude with the real-scale have been conducted in view of addressing the interaction between the flow and the barrier. A particular attention was paid to the identification of the parameters with influence on the loading experienced by the barrier, varying the woody debris mixtures characteristics, water discharge, flume inclination and woody debris supply mode. This investigation emphasized the intricacy of the relation between the barrier loading and the characteristics of the trapped logs and of the logs accumulation. The barrier loading revealed inversely proportional to the woody debris accumulation permittivity, which quantifies its capacity to let the water seep through. Permittivity depended on the way the accumulation built up and on the evolution of its characteristics with increasing discharge and trapped logs volume. Finally, the loading exerted by the flow on the barrier was derived from the barrier elongation, revealing that it could be modelled as a hydrostatic load with a reduction factor of 0.5.

Keywords: driftwood, flood, flexible barrier, flume experiment, loading

1 Introduction

25 Large wood pieces transported by flows, also called in-stream wood or woody debris, pose serious problems when driven in rivers and torrents (Fig. 1). Woody debris observed in thalweg may be generated by events such as landslides and bank erosions, as well as eventually forest fires, snow avalanches or the flooding of anthropogenic deposit, e.g. after logging

operations (Gasser et al., 2019). When water flows with sufficient intensity, woody debris are transported and may accumulate on bridge piers or water intake, or be blocked in river sections with reduced width leading to flooding of vulnerable areas (Lucia et al., 2015; Comiti et al., 2016 ; Ruiz-Villanueva et al., 2014, 2019 ; Okamoto et al., 2020).



Figure 1: Woody debris accumulations upstream bridges in close vicinity to elements at risk (Lucia et al., 2015).

35 The best option to prevent woody debris accumulation (or jam) at critical locations, such as a bridges and dams, is often to adapt the structure to make it sufficiently wide and flowing over a depth allowing the debris to be transferred downstream (ICOLD, 2019). In many cases, such adaptations are not possible and the mere width of the river and roughness of the banks is prone to create woody debris jams. In such cases, it becomes necessary to trap woody debris with dedicated civil engineering structures built upstream vulnerable areas.

40 Rigid structures made of concrete, grills and posts are traditionally used to trap woody debris along with sediment in torrents and small rivers (Schmocker and Hager, 2013; Piton and Recking, 2016). As illustrated in Figure 2, flexible barriers made of cable supported steel nets have been more recently proposed as a cost saving alternative for retaining woody debris (Rimböck and Strobl, 2002; Rimböck, 2004; Lambert et al., 2023; Piton et al., 2023). Flexible barriers are widely used in torrents for containing debris flows (Wendeler and Volkwein, 2015; Wendeler, 2016; Berger, 2021) and many research have addressed

45 the debris flow pile up and the resulting barrier loading (Ng et al., 2016; Albaba et al., 2017; Wendeler et al., 2019; Choi and Goodwin, 2020; Tan et al., 2020; Kong et al., 2023). A recent comprehensive literature overview on the impact loading exerted on flexible barriers used in this purpose can be found in Kong et al. (2022). The interception of logs and their accumulation against man-made structures has received substantial interest with application to bridges, piers and trapping structures and in particular over the recent years (Rimböck and Strobl, 2002; Rimböck, 2004; Lange and Bezzola, 2006; Schmocker and

50 Weitbrecht, 2013; Schalko et al., 2019a, 2019b; Okamoto et al., 2019; Cicco et al., 2020; Piton et al., 2020). The interception

leads to an accumulation of logs which results in an increase in water depth upstream the accumulation (also referred to as backwater rise), and eventually in a local scour below the accumulation (Schalko et al., 2019a, 2019b).

To the author's knowledge, the use of flexible barriers for containing woody debris has received very limited attention, while these structures significantly differ by their high porosity and flexibility. The only exception concerns the research presented by Rimböck and Strobl (2002) and by Rimböck (2004) that defined the field of application of flexible trapping barriers and proposed a design method based on experiments including full-scale tests on a prototype barrier.



60 **Figure 2: Woody debris trapped in flexible barriers in New Zealand (a) and in the USA (b) (Courtesy of Geobrugg and KANE GeoTech Inc respectively) and in the preliminary flume experiments with a smaller net with thin logs (c) and thick logs (d)**

In order to further investigate the use of flexible barriers for trapping woody debris, the authors have very recently conducted flume experiments at a scale ratio of 1/40 (Lambert et al., 2023; Piton et al., 2023). One major finding was that flexible barriers are more efficient than more conventional civil engineering structures for intercepting woody debris in particular due to their larger porosity. Indeed, the net minimize the upstream flow level by allowing water to seep through all the structure (as opposed

to a concrete dam with smaller openings) and the mesh entangle woody debris and prevent their release even in case of flow passing over the top cable.

In an innovative way, the flexible barriers used for these small-scale experiments were designed in view of having both geometrical and mechanical similitude with the real-scale (Lambert et al., 2023). In this purpose, the 3D printing technique
70 was used for manufacturing the barrier. Tests were conducted varying the barrier height, barrier bottom clearance, woody debris mixture characteristics, woody debris supply mode, water discharge and flume inclination. Piton et al. (2023) pooled all these data in a single dataset and mainly interpreted and discussed the results in terms of trapping efficiency and hydraulics, i.e. rise in the water depth upstream of the barrier (backwater rise).

Based on these experiments, the authors observed that, similarly as observed by other authors (Rimböck and Strobl, 2002;
75 Lange and Bezzola, 2006), the logs accumulate upstream the barrier in such a manner that can be schematically described as a log plug along the structure complemented with a carpet of floating logs near the water surface (

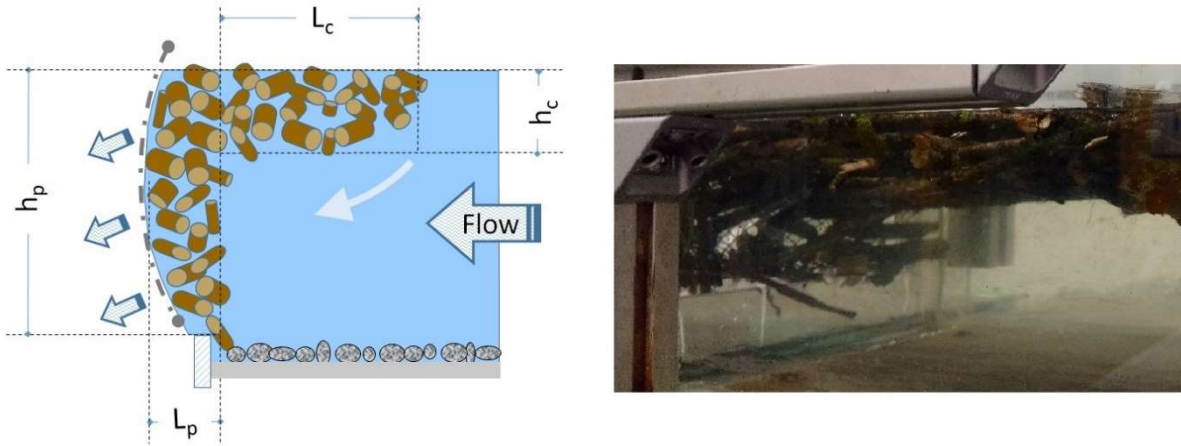
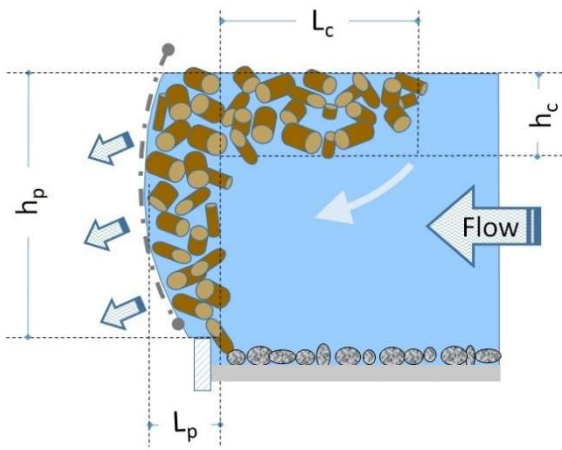


Figure 3). The backwater rise induced by this accumulation results in an increase of the load applied on the barrier. The mechanisms governing the load transfer to the barrier, depending on the configuration, has however not been addressed to the
80 best of our knowledge. The lack of specific knowledge in particular concerns the amplitude and spatial distribution of this loading, for a given context in terms of discharge and trapped woody debris.



85 **Figure 3: The logs accumulation upstream the barrier consists of a plug along the barrier and a floating carpet which are schematically defined, for the purpose of this study, by their height and length: (h_p , L_p) and (h_c , L_c) respectively. Example of logs accumulation upstream a flexible barrier exhibiting a long carpet (experiments presented in Piton et al. 2023).**

In view of contributing to the improvement of the structural design of these barriers, this article provides a detailed description of the interaction between a flexible barrier and flow-driven woody debris and discusses the mechanisms at work, focusing on the loading applied on the barrier. In this aim, the results from 54 small-scale experiments conducted in the lab and previously introduced by the authors are considered (Piton et al, 2023). The interaction between the flow and the barrier is addressed considering measurements of the barrier deformation and backwater rise and an estimation of the woody debris accumulation permittivity. First, a reference test is considered for describing this interaction while increasing the discharge and the volume of supplied woody debris. Then, the changes induced by varying the woody debris supply mode, flume inclinations and woody debris mixture characteristics are successively addressed. The results provide deep insights into the interaction between the barrier and the flow. The loading on the barrier is derived from the barrier elongation, revealing that it could be modelled as a hydrostatic load with a reduction factor of 0.5.

2 Materials and methods

2.1 Flume

100 The tests were conducted in a 6 m long flume, 300*400 mm in cross section (height*width). Water was pumped into the flume at a maximum discharge of 8 l/s. The discharge was measured by an electromagnetic flow meter, with a 1% accuracy. A layer of gravel 15-20 mm in grain size covered the channel bottom and a 10 mm thick Plexiglas sheet with a 300 mm in width opening was placed at its extremity. The gravel size was determined to introduce roughness while avoiding scour during the experiments.

105 The flume was equipped with an ultrasonic sensor placed above the water and 200 mm in distance upstream the barrier (**Figure 4**). This distance was required to prevent from any measuring bias associated with logs significantly protruding from the water surface at very close proximity to the barrier. This sensor allowed determining the water depth with an accuracy of ± 2 mm.

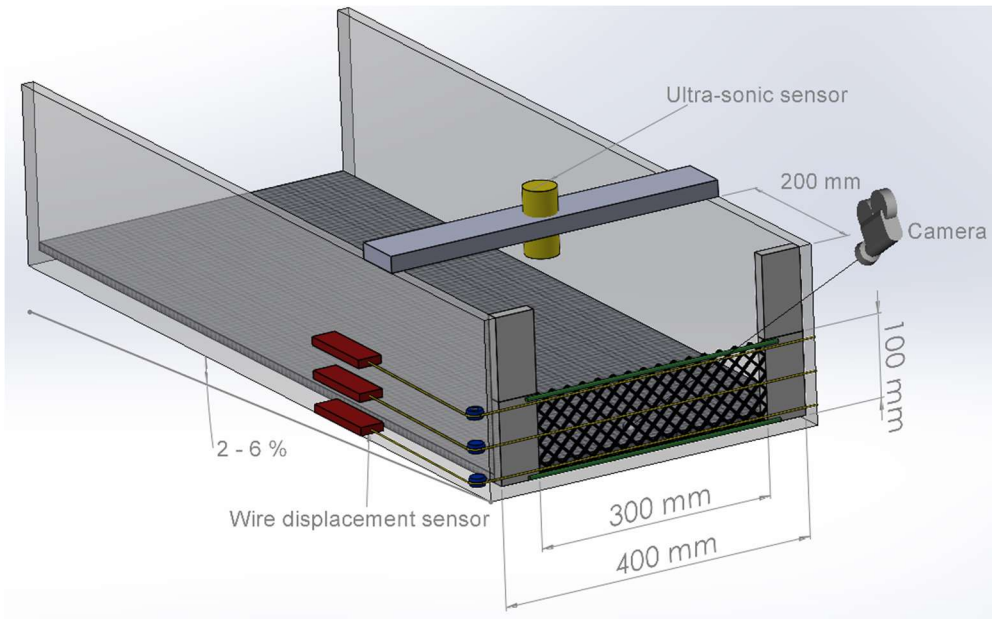
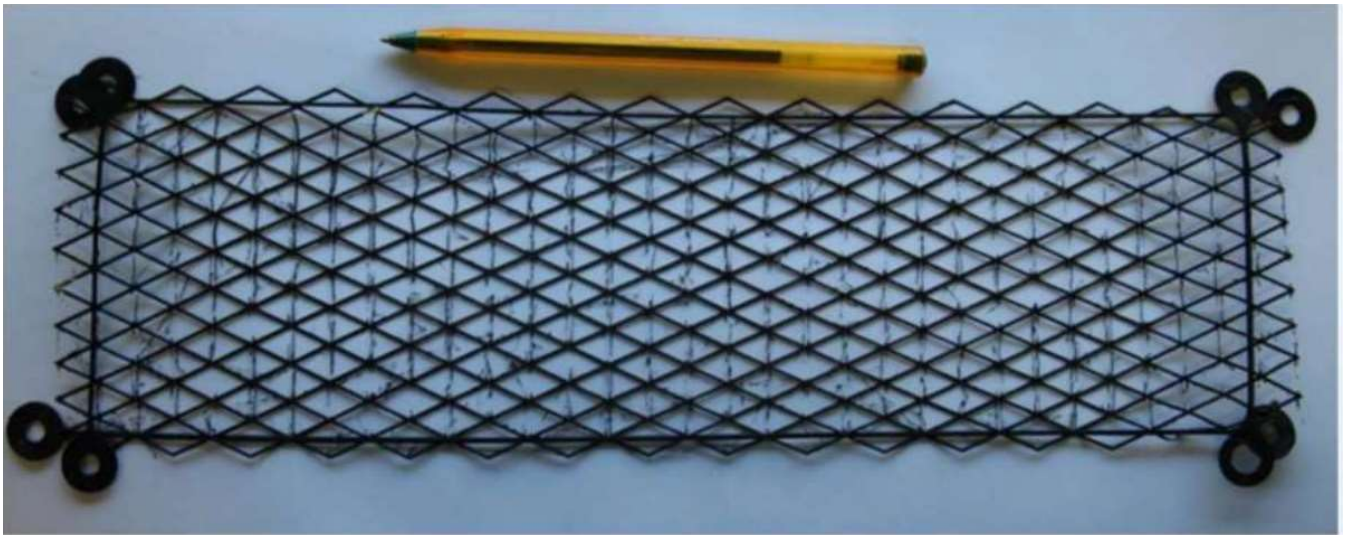


Figure 4: Sketch showing the flume, barrier and sensors

110

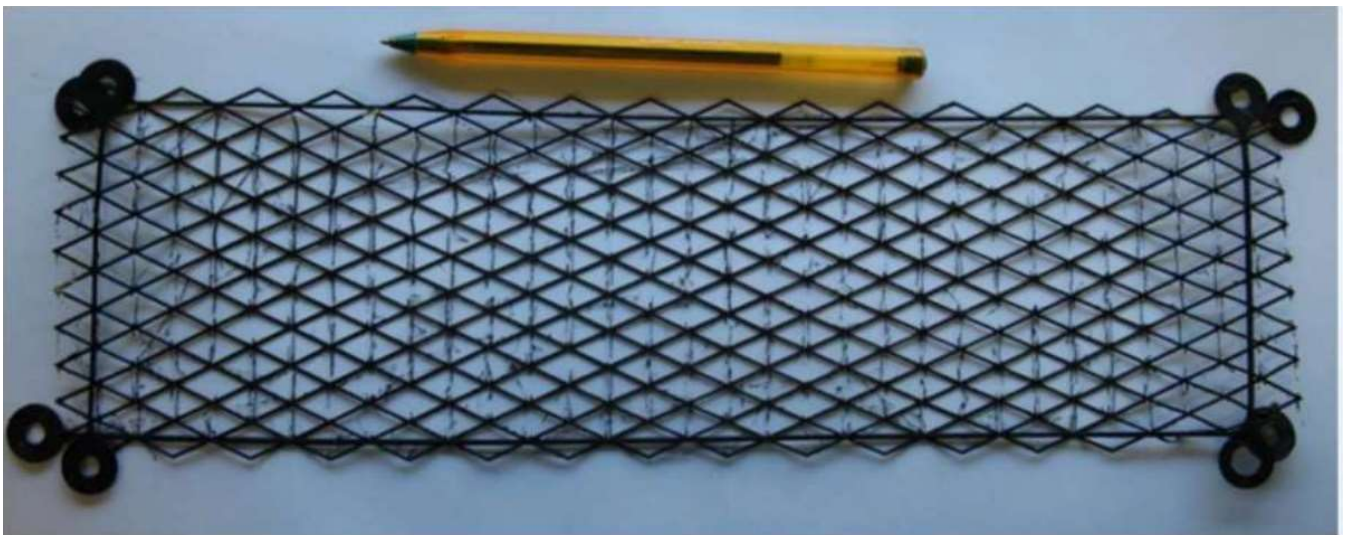
2.2 Flexible barrier

The flexible barriers used for these experiments were designed to correspond to current practices. They consisted in an interception net with a diamond-shape mesh that was supported by two cables along its upper and lower edges and laterally fringed by two cables along the vertical edges (



115

Figure 5). These cables were interlaced with the net to insure connection. By contrast with most of real structures, the barrier did not integrate energy dissipation devices (also referred to as brakes) to enable an analysis strictly focusing on the barrier deformation, from which the loading could be derived.



120

Figure 5: The considered barrier consists of a mesh bordered with four cables. Eyelets at the cables extremities allow securing the barrier at the flume extremity.

The extremities of the four cables were equipped with eyelets to secure the barrier on screws passing through the Plexiglas
125 sheet. In this manner, the cables always had the same position and tension from one test to the other.

A particular attention was paid to similitude issues designing the barrier (Lambert et al., 2023). The dimensions and mechanical characteristics of the barrier components were determined to have similitude with a real barrier 40 times larger. Notably, the barrier was given mechanical characteristics such that its deformation under normal-to-the-plane loading matched that at the real-scale under the same loading. This was achieved by the 3D printing technique, after selecting the polymer with appropriate tensile stiffness. The mechanical characteristics of the cable and net are given in Lambert et al. (2023). The net was 100*300 mm in dimensions and the supporting cables were 330mm long. The unit mesh had a diamond-shape, 9.4 mm by 20.6 mm in dimensions.

The barrier deformation along the longitudinal axis was measured thanks to three wire displacement sensors with a 0.1 mm resolution. These wires were placed along the lower barrier cable, at barrier mid-height and along the top barrier cable. Specific tests on the barrier used in this study revealed that its mid-height deformation reached 40 mm when exposed to a hydrostatic pressure with a 100mm water head, i.e. corresponding to the barrier height. For more details, see Lambert et al. (2023) and Piton et al. (2023).

2.3 Woody debris mixtures

Four woody debris mixtures were considered in this study (Table 1). These mixtures are those presented in Piton et al. (2023) on which flume experiments included the measurement of the barrier deformation. Considering their dimensions and the scale ratio of these lab experiments, these logs correspond to Large Woods (LW) at the real-scale. Pine needles were added to mixture labelled as “B” to mimic small flexible branches as opposed to the log representing trunks and thick, rigid branches. The mixtures differed by the log mean diameter, log mean length, content in fine material (pine needles) and total volume supplied. Piton et al. (2023) gave a more detailed description of these materials. Each of these parameters was suspected to potentially play a role in the interaction between the water flow loaded with woody debris and the flexible barrier (Schalko et al., 2019a). Indeed, these parameters have an influence on the logs accumulation porosity and logs interlocking. It was expected that these different mixtures could result in difference in loading on the barrier, and thus in differences in barrier deformation. Mixture 3B will be considered first to investigate the influence of the supply mode, discharge and slope. Then, the influence of the supplied material will be investigated considering all four mixtures. By comparison with mixture 3B, mixtures 1A and 2A contained no pine needle, their total volumes were half that of the former and have varied maximum log length. Mixture 6B consisted of slightly thicker and shorter logs than mixture 3B. The differences in logs number result from the difference in total volume, log length and diameter.

155

Table 1: Woody debris mixtures

Mixture	Number of logs	Mean log length, Lw (mm)	Max. log length, Lmax (mm)	Mean log diameter, dw (mm)	Total volume (10 ⁻³ m ³)	Fine material
1A	246	87	200	7.8	1.04	No
2A	250	67	150	6.2	0.94	No
3B	507	82	200	7.4	2.04	Yes
6B	320	66	100	11.8	2.29	Yes

2.4 Woody debris supply

The log transport in torrents globally increases with water discharge, but log supply at the barrier location is very stochastic, varies greatly between events and is always unknown to the barrier designer. In addition, it was suggested to have an influence on the barrier response (Rimböck and Strobl, 2002). For these reasons, three different supply modes were considered in this study while increasing water discharge by 1 l/s steps from 0 to almost 8 l/s.

The first mode, referred to as 1-1, consisted in placing all the logs in the flume at the beginning of the first phase. The second and third modes, referred to as 1-3 and 1-7 respectively, consisted in progressively supplying the logs while increasing the discharge by steps: 1/3rd of the logs supplied during the first three steps and 1/7th of the logs during each of the seven successive steps respectively. The logs were supplied at a 500 – 2000 mm distance upstream the barrier, randomly but generally quite evenly distributed in the flume width.

These three different modes correspond to very different scenarios of logs transport observed in torrents. The first mode corresponds to the case where a great number of woody debris are available in the torrent bed before the flood, while the two others correspond to cases where woody debris are recruited on the banks with increasing water depth and associated erosion.

2.5 Test campaign and data treatment

The tests were performed considering three flume inclinations: 2, 4 and 6% (corresponding to angles of 1.15, 2.3 and 3.4° approx.). In the absence of woody debris, the Froude number was measured to range from 0.5 to 0.65 for the 2% inclination while values of 1 and 1.4 were obtained when the flume was inclined by 4 and 6% respectively. These values are in accordance with actual Froude numbers in torrents (Piton and Recking, 2019).

The discharge, water depth and barrier elongation were recorded continuously during the tests at a 10 Hz frequency. In addition, pictures showing the barrier and water surface were taken each 10 seconds. These images were useful to interpret sensor data and in particular revealed the barrier global deformation and the accumulation of logs at the water surface.

Each discharge step lasted about 3 minutes to reach a stable situation. The increase in discharge induced a variation in all measures, with a rapid evolution with time before reaching a plateau, indicating that stability was achieved. The response of the system (consisting in the trapped logs and the barrier) was determined from averaged values out of the data collected over this plateau.

Table 2 lists the various test performed and mentions the test conditions (mixture, slope, supply mode and maximum discharge) and main results (maximum flow depth, maximum barrier elongation at mid-height and permittivity at maximum discharge). The presented results are averaged values out of the three repetitions that were conducted for each test configuration. Table 2 also shows the standard deviation.

Table 2: Tests conditions and main results

Test ID	Mixture	Slope (%)	Supply mode	Maximum discharge, Q_{max} ($l.s^{-1}$)	Max. depth (mm)	Max. elongation, at barrier mid-height (mm)	Permittivity, $P_{Q_{max}}$ (s^{-1})
3B_2.1	3B	2	1-1	7.5	102 ± 5	12.5 ± 0.8	4.2 ± 0.4
3B_2.3	3B	2	1-3	7.6	109 ± 3	14.3 ± 1.2	3.7 ± 0.3
3B_2.7	3B	2	1-7	7.7	115 ± 0.3	12.5 ± 2.4	3.3 ± 0.3
3B_4.1	3B	4	1-1	7.2	116 ± 1	20.7 ± 2.3	2.5 ± 0.2
3B_4.3	3B	4	1-3	7.0	117 ± 2	18.9 ± 2.4	2.4 ± 0.2
3B_4.7	3B	4	1-7	6.9	119 ± 1	15.8 ± 2.6	2.2 ± 0.2
3B_6.1	3B	6	1-1	7.2	117 ± 9	15.7 ± 1.5	2.3 ± 0.2
3B_6.3	3B	6	1-3	7.4	128 ± 2	18.8 ± 1.2	1.9 ± 0.1
3B_6.7	3B	6	1-7	7.4	122 ± 1	18.5 ± 2.2	2.1 ± 0.2
1A_2.1	1A	2	1-1	7.7	88 ± 3	12.4 ± 1.4	7.1 ± 0.9
1A_2.3	1A	2	1-3	7.7	91 ± 4	10.6 ± 1.6	6.4 ± 0.7
1A_2.7	1A	2	1-7	7.7	93 ± 2	11.4 ± 0.7	5.9 ± 0.6
2A_2.1	2A	2	1-1	7.6	90 ± 3	13.5 ± 0.1	6.6 ± 0.8
2A_2.3	2A	2	1-3	7.6	92 ± 1	13.1 ± 2.6	6.1 ± 0.7
2A_2.7	2A	2	1-7	7.6	94 ± 4	13.7 ± 1.3	5.6 ± 0.6
6B_2.1	6B	2	1-1	7.6	82 ± 3	10.6 ± 0.6	8.7 ± 1.3

6B_2.3	6B	2	1-3	7.4	80 ± 6	10.1 ± 1.5	9.4 ± 1.4
6B_2.7	6B	2	1-7	7.4	88 ± 3	12.4 ± 1.4	7.1 ± 0.9

190 The last column shows the permittivity (s^{-1}) at maximum discharge computed following Eq.1 (Faure et al., 1999):

$$P_{Qmax} = \frac{Q}{A \cdot h^*} \quad (1)$$

With Q the discharge ($m^3 \cdot s^{-1}$), A the area through which water flows out of the flume (m^2) and h^* (m) the backwater rise. These latter are computed following Eq.2 and 3:

$$A = h \cdot b \quad (2)$$

195 $h^* = h - h_0 \quad (3)$

With b (m) the width of the rectangular opening at the flume extremity, h (m) the water depth measured upstream the barrier when the flow was loaded with woody debris and h_0 (m) the water depth measured upstream the barrier with pure water, at the same discharge.

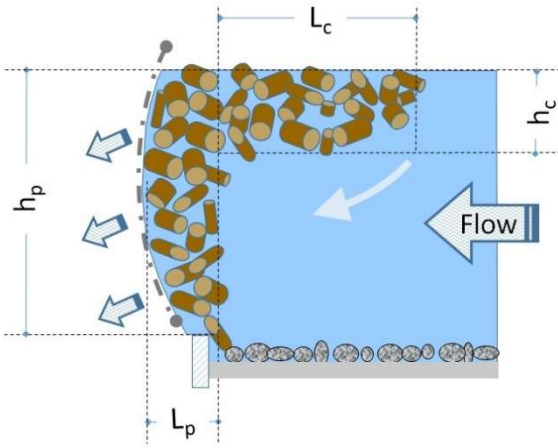
200 Considering the findings presented in Piton et al. (2023), h_0 was computed as the water depth at a weir where approaching flows have non-negligible inertia term following Eq. 4:

$$h_0 = \frac{1}{1 + \frac{Fr_0^2}{2}} \sqrt[3]{\frac{Q^2}{2g \cdot \mu^2 \cdot b^2}} \quad (4)$$

With μ the weir coefficient (equalling 0.45 in this case), g the gravity acceleration ($m \cdot s^{-2}$), and Fr_0 the Froude number (-), which values for the three different slopes considered have been given previously.

205 Permittivity is a proxy of the ability of the logs accumulation upstream the barrier to let the water seeping through. Permittivity was preferred over permeability for revealing the evolution in hydraulic characteristics of the logs accumulation because permeability requires determining the dimension of the logs accumulation in the flow direction while this value was hard to

determine and variable with flow conditions (



210 Figure 3).

As test 3B_4.3 presents intermediate slope inclination and supply mode, it was considered as the reference case when evaluating the influence on the barrier deformation of the flume inclination and log supply mode. The investigation of the influence of the woody debris mixture characteristics is based on tests conducted at a 2% inclination for the four different mixtures because only mixture 3B was employed in tests at different inclinations.

215 3 RESULTS

3.1 System response

3.1.1 Response to increasing discharge and amount of woody debris

Case 3B_4.3 was considered for describing the evolution of the woody debris accumulation, backwater rise and barrier deformation from the test beginning to its end.

220 At the very first discharge step (1 l/s) only a fraction of the logs reached the barrier after supply (Figure 6: b). In fact, part of the logs remained blocked on the gravel bed due to insufficient water depth and flow velocity in the flume area where logs were supplied. Logs were progressively recruited increasing discharge and reached the barrier (Figure 6: c). In Figure 6: d, all the logs were supplied and accumulated near the barrier. Interestingly, increasing further the discharge led to the decrease in the length of the logs accumulation at the water surface suggesting an increase in density of the logs accumulation (Figure 6: d vs Figure 6: e).

225

During the tests, the orientation of logs at the surface and near the barrier were mostly horizontal and perpendicular to the water flow direction (Figure 6:). However, the orientation of logs further from the barrier and close to the flume walls deviated

with respect to the flow direction. Some non-horizontal logs close to the barrier favoured interlocking between superimposed logs that piled-up.

230

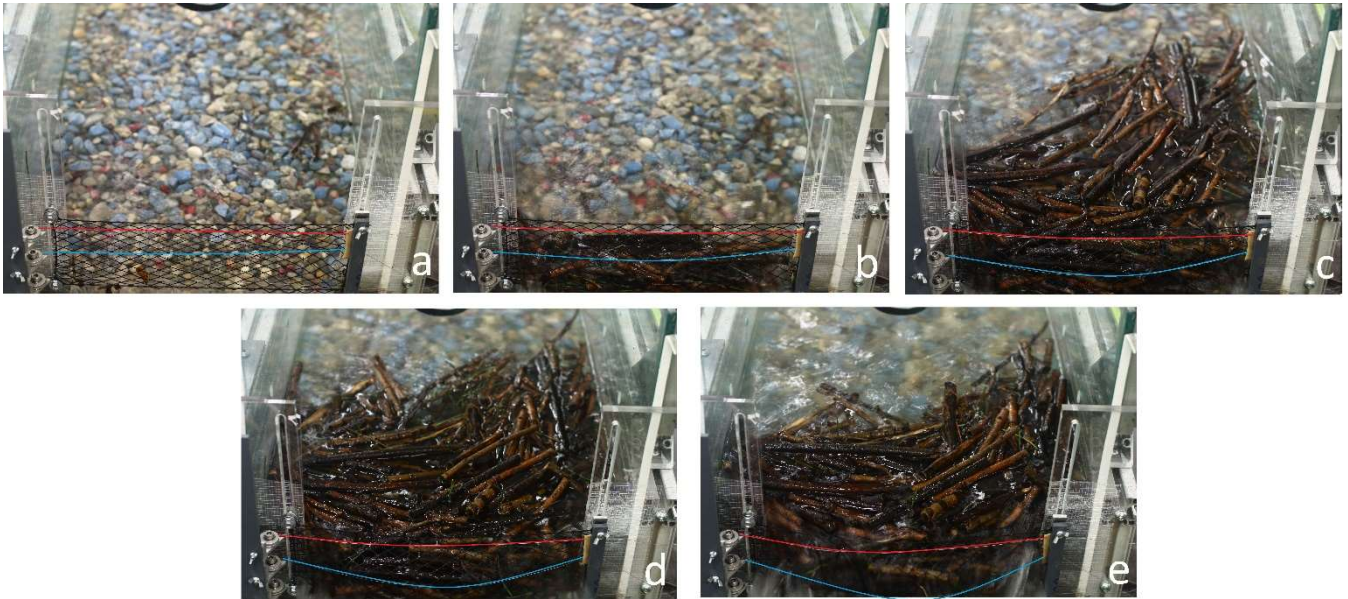
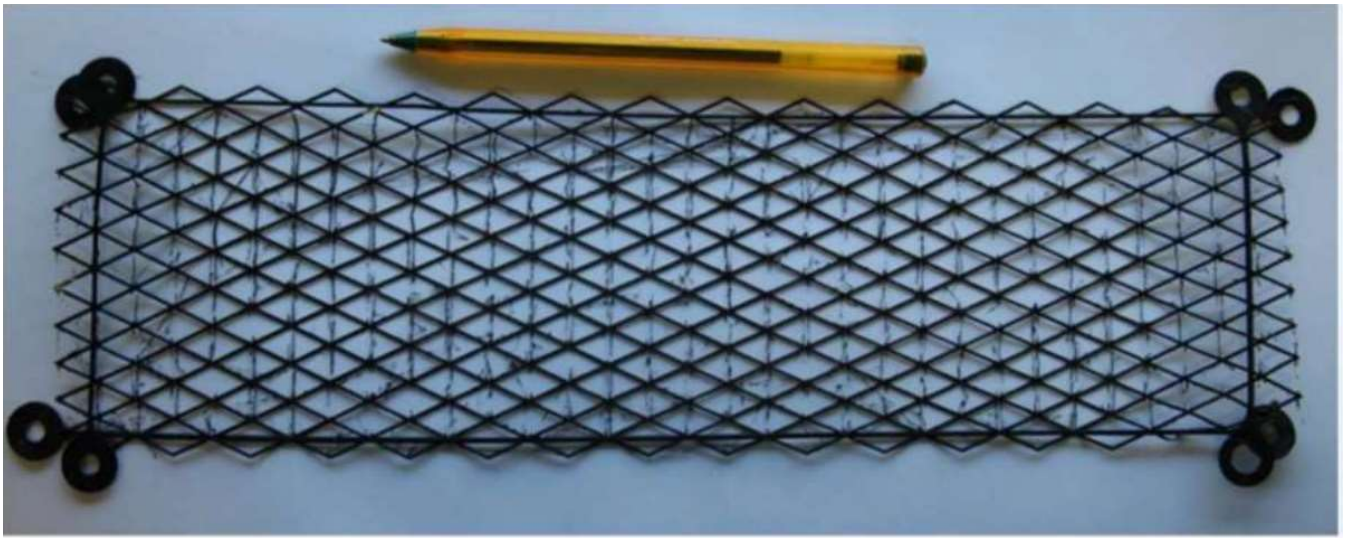


Figure 6: View of the barrier and logs accumulation during test 3B_4.3 c: (a) beginning, (b) 1 l/s discharge and 1/3 of the logs supplied (c) 2 l/s discharge and 2/3 of the logs supplied, (d) 3 l/s discharge and all the logs supplied and (e) maximum discharge). The blue and red curves show the position of the mid-height and top sensor wires respectively.

235

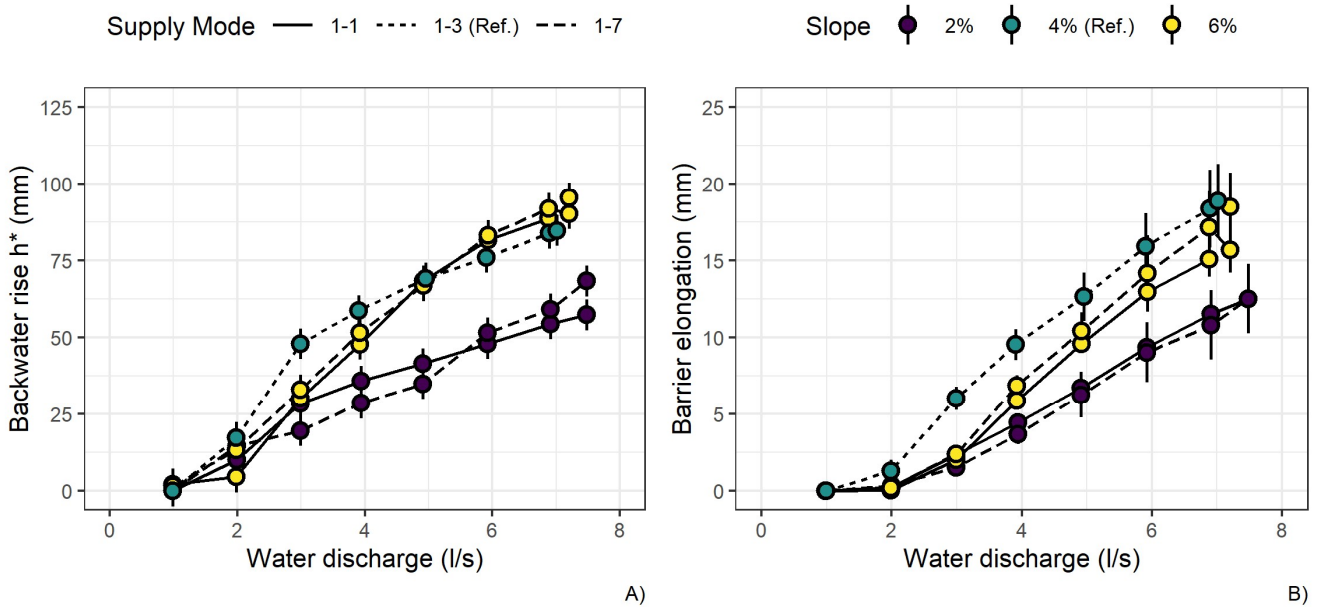
The increase in water depth was higher during the first steps, when the logs were supplied (Figure 7:). The elongation measured by all three sensors revealed a monotonous increase with increasing discharge. The elongation measured at barrier mid-height was much higher than that at the top and bottom of the barrier, which was due to the absence of barrier cable at mid-height as shown in



240

Figure 5. The elongation at the bottom and mid-height of the barrier initiated from the first step. By contrast, the upper part of the barrier started experiencing deformation above a 3 l/s discharge. This discharge corresponded to a 65 – 70 mm water depth approximately, revealing that load transferred within the net from the lower part of the barrier to the top barrier-supporting cable. At maximum discharge, the elongation measured along this latter cable was about 40% less than that along the lower barrier cable. Large variability in elongation was observed at barrier mid-height within the three repetition tests as illustrated by the standard deviation bars.

245



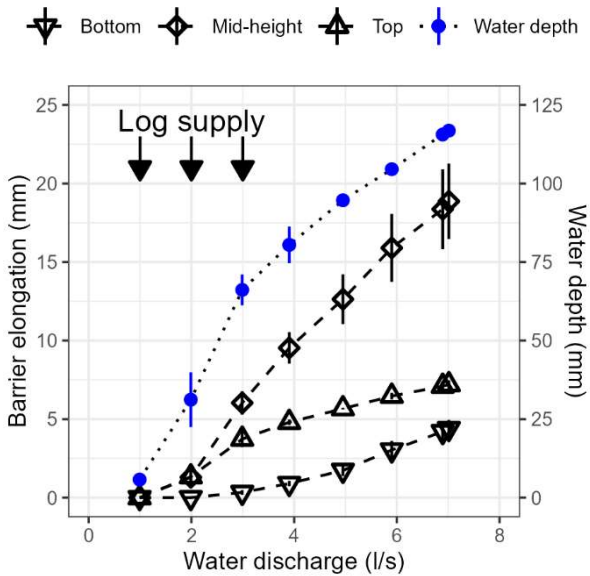
250 **Figure 7: Main measurements during the test with mixture 3B, with a 4 % flume inclination and supplying logs in three times (test 3B_4.3).**

255 The water depth measured upstream the barrier at the end of the test sequence was higher than the barrier initial height (almost 120 vs. 100mm) which was partially due to logs accumulation above the top cable, by a few centimetres. Interlocking of these logs with logs below prevented them from being driven downstream. This is consistent with observations in the field (Figure 2 a,b).

3.1.2 Response varying the log supply mode and flume inclination

The evaluation of the influence of the supply mode and flume inclination was addressed considering mixture 3B and focusing on the four extreme situations regarding slope and supply mode, which relate to tests 3B_2.1, 3B_2.7, 3B_6.1 and 3B_6.7. The comparison was based on the backwater rise, h^* , and on the elongation at barrier mid-height (Figure 8).

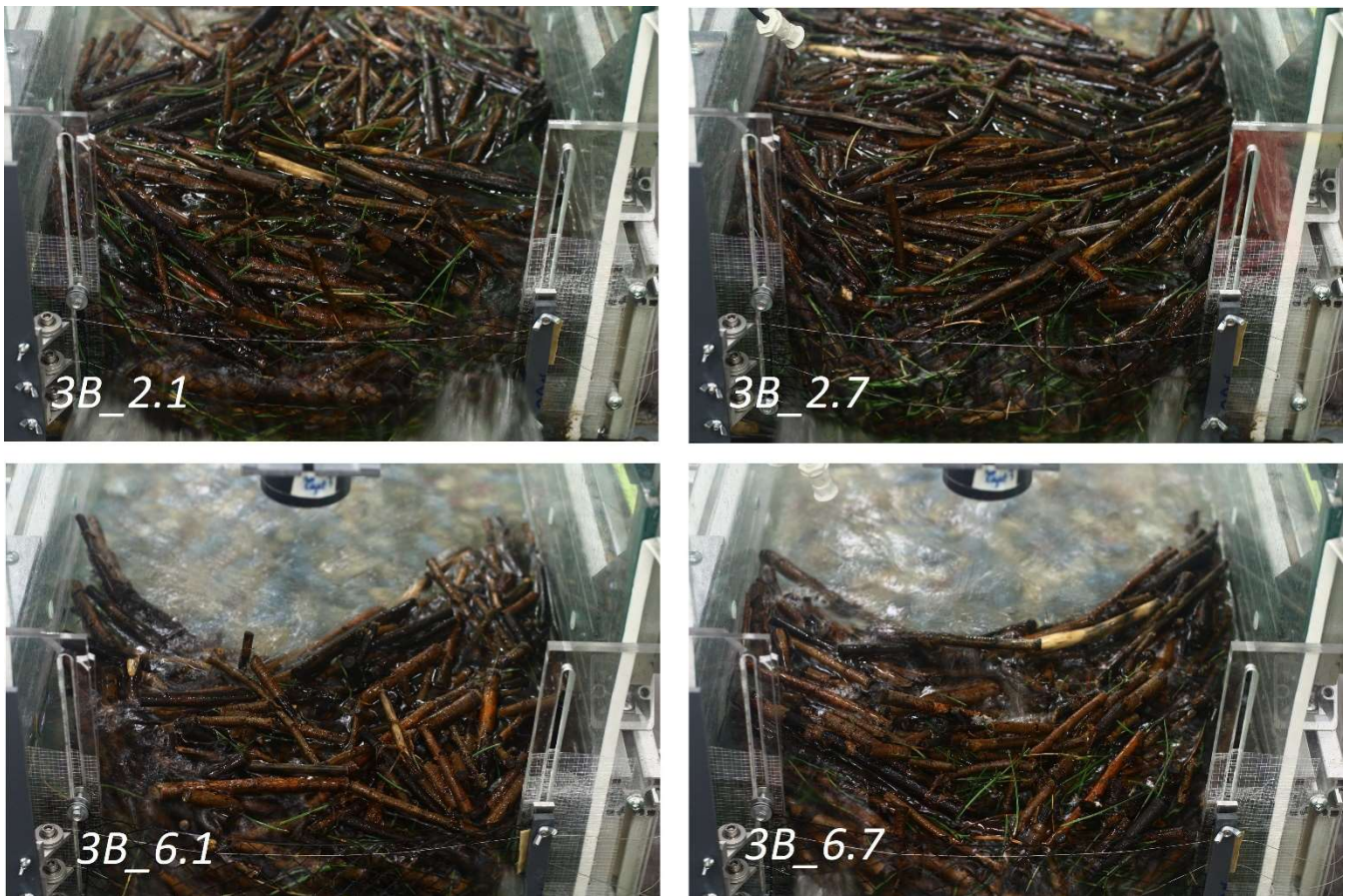
260 The system response showed a clear dependence on the flume inclination. An increase in flume inclination from 2 to 6% led to an increase in both the backwater rise, h^* , and the elongation at barrier mid-height, by about 35 and 50 % at the highest discharge respectively (Figure 8). By contrast, the supply mode had a much lower influence on the backwater rise and barrier elongation measured along the test.



265 **Figure 8: Backwater rise, h^* (left) and elongation at barrier mid-height (right) with a flume inclined by 2 and 6% and supplying mixture 3B in one or seven times and comparison with the reference case (3B_4.3).**

Results obtained with a 6% flume inclination were much closer to that from the reference test (3B_4.3). The main differences
270 concerned the measurements at low discharge values. The difference between cases 3B_4.3 and 3B_6.7 was attributed to the
fact that, in the latter case, logs were progressively supplied increasing discharge. The difference in supply mode also explained
the difference observed between test 3B_4.3 and test 3B_6.1 as, in this latter case, logs remained blocked on the gravel bed
before a sufficient discharge was reached (typically 3 l/s). In both cases, the number of logs trapped by the barrier during the
275 first stages of the test was higher for the reference case, with mode supply 1.3, resulting in higher backwater rise and barrier
elongation.

Visual observations revealed a general trend where the length of the logs accumulation at the water surface decreased as the
inclination increased (top vs bottom pictures in Figure 9:) and that the tail of the carpet was less dense with a 2% inclination.
This was attributed to the higher incoming water flow mean velocity, i.e. upstream and under the floating carpet, and it suggests
that the accumulation was denser and, possibly, the accumulation mainly consisted in a plug. This would be consistent with
280 the conclusions drawn from Figure 8, in terms of backwater rise and barrier elongation. By contrast, the supply mode did not
seem to have an influence on the length of the logs accumulation at the water surface (pictures at the right vs pictures at the
left in Figure 9:).

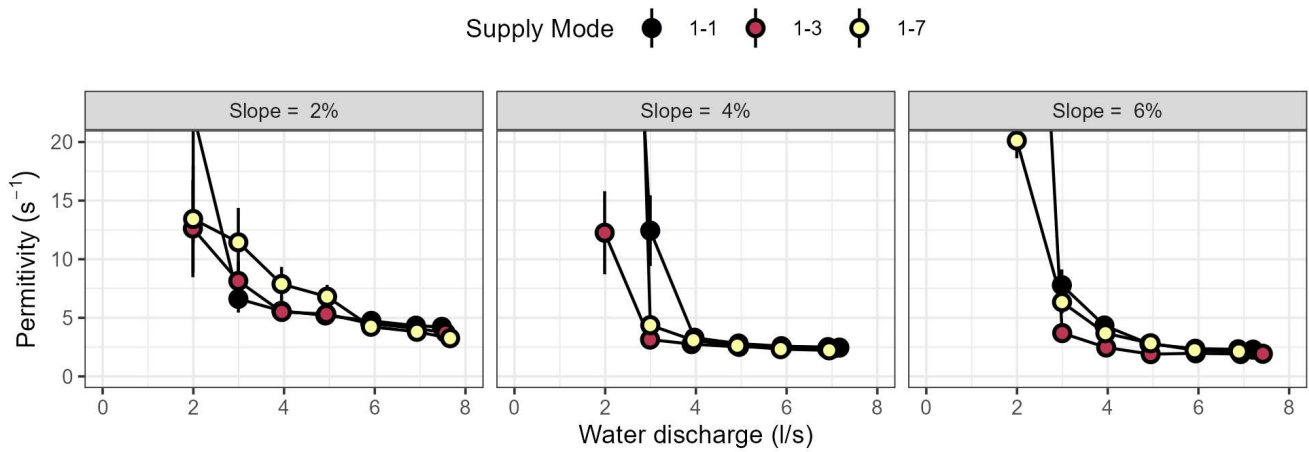


285 **Figure 9: Logs accumulation at the flow surface at maximum discharge during tests with mixture 3B, in a flume inclined by 2 and 6% and supplying mixture the logs in one or seven times.**

The variation in water depth with increasing discharge as well as the differences in backwater rise at maximum discharge between the different situations, draw the attention on the permittivity of the logs accumulation along the tests for the different supply modes and flume inclinations (Figure 10:). Due to the insufficient mobility of logs below a discharge of 3 l/s and the uncertainty in the estimated water depth of the pure water flow, h_0 , the mean values at discharges up to 3 l/s were most often not reliable.

290 The general trend for all supply modes and flume inclinations was a decrease in permittivity with increasing discharge, as well as with increasing volume of logs supplied. When the flume was inclined by 4 or 6%, a plateau was reached above a 5 l/s discharge, whatever the supply mode. Above this discharge, the different supply modes resulted in very similar permittivity values, in particular for the 4% flume inclination. By contrast, permittivity exhibited a decreasing trend up to the highest

discharge when the flume was inclined by 2%, with a final value significantly higher than that observed for the two other inclinations.



300

Figure 10: Permittivity variation with increasing discharge supplying mixture 3B in one, three and seven times (1-1 to 1-7) in a flume inclined by 2, 4 and 6%

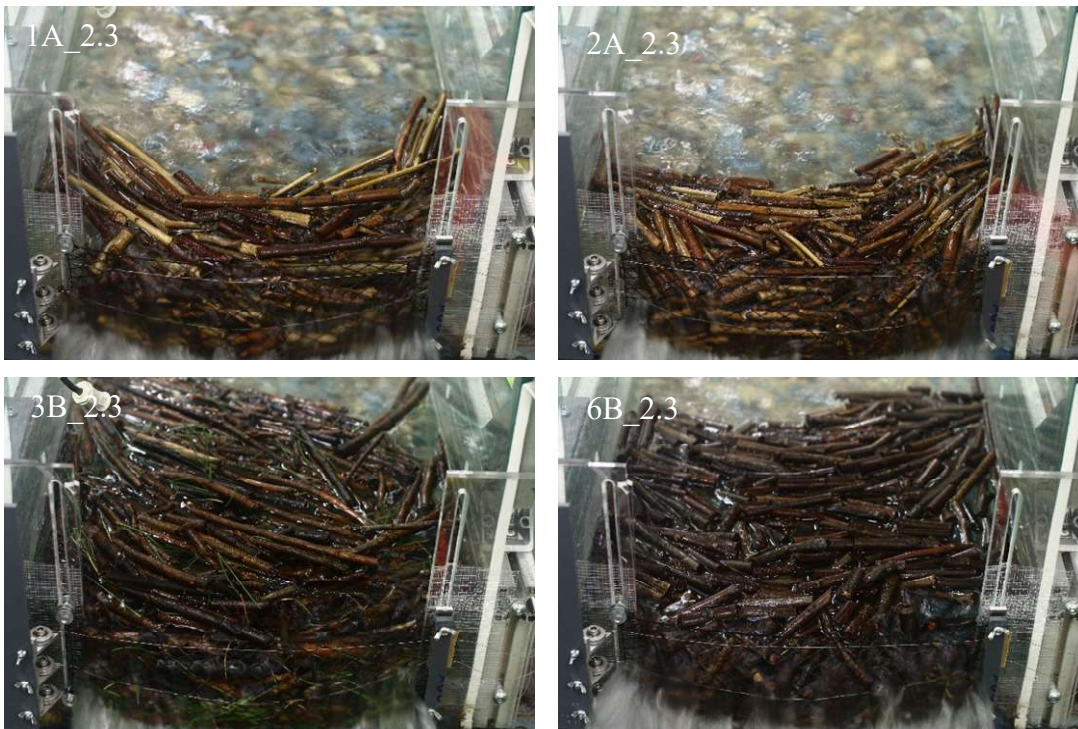
3.1.3 Response varying the log mixture characteristics

305

The trends observed with mixture 3B in terms of barrier elongation and water depth while increasing discharge were consistently observed with mixtures 1A, 2A and 6B (see Appendix A). Tests with these mixtures considered a 2% flume inclination only. The influence of the mixture is addressed considering the measurements at the end of the tests, which are highly relevant in a barrier design perspective.

310

The main visual observation was that mixtures 1A and 2B resulted in shorter logs accumulation at the water surface compared to mixtures 3B and 6B (Figure 11:). This is most likely an effect of the almost doubled volume of logs in the latter group of mixture than in the first one. Changing the log diameter (compare mixtures 3B and 6B) or the log length (compare mixture 1A and 2A) has marginal influence on the logs accumulation. More specifically to mode supply 1-1, mixture 6B resulted in slightly shorter logs accumulations at the water surface than mixture 3B which is likely an effect of the shorter length of the logs that more easily rearrange and pack more densely.



315

Figure 11: Logs accumulation at the flow surface at maximum discharge during tests in a flume inclined by 2% supplying mixtures 1A, 2A, 3B and 6B in three times (from top left to bottom right) .

In terms of elongation at barrier mid-height, the difference between the mixtures was negligible for supply mode 1-7 (Figure 320 12:). This is likely an evidence that when the logs accumulation build up progressively, the logs self-organize in a way that distribute the forces within the pack irrespective of the size and number of logs. Conversely, a higher difference between the mixtures emerged with supply modes 1-1 and 1-3, where the highest elongation values are at least 30% higher than the lowest ones. For these tests, the logs were supplied more suddenly and the packing is likely more influenced by the random position that cluster of logs had when reaching the barrier. The highest difference in elongation was observed between mixtures 6B and 325 3B for supply mode 1-3, with a 40% difference.

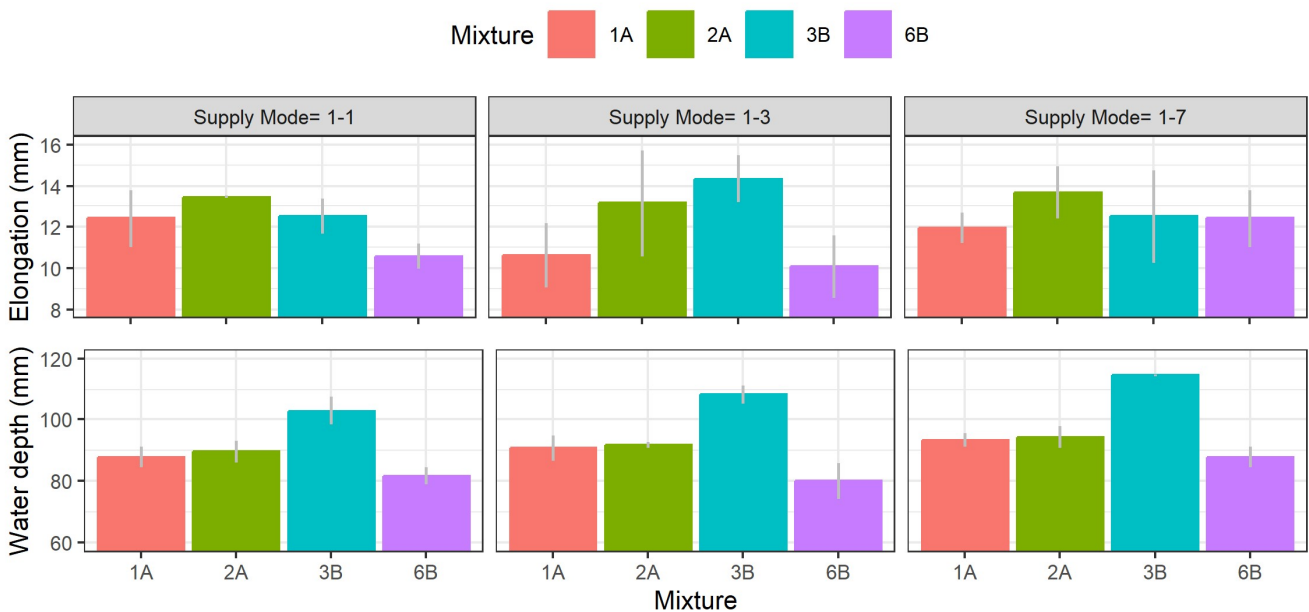


Figure 12: Elongation at barrier mid-height and water depth at maximum discharge, for the different mixtures and supply modes, in a flume inclined by 2%.

330

In terms of water depth at maximum discharge, differences were observed between the four mixtures. Highest and lowest values were obtained with mixtures 3B and 6B, respectively. For all mixtures, the water depth tended to slightly increase from supply mode 1-1 to supply mode 1-7. We also interpreted this as a tendency to build denser pack when the supply was progressive and the pack might adjust and rearrange under increasing flow intensity.

335

Interestingly, mixtures 1A and 2A exhibit very similar water depth values, for all supply modes, but mixture 2A resulted in globally higher elongation values suggesting that the resistance opposed to flow within the pack, which is associated with the water depth, and the transfer of forces to the barrier, which is revealed by its elongation, are partially independent.

Trends observed with mixtures 1A, 2A, and 6B in terms of permittivity variation increasing discharge and volume of supplied logs (see Appendix B) were very similar to that observed during 2% flume inclination tests with mixture 3B (Figure 10:).

340

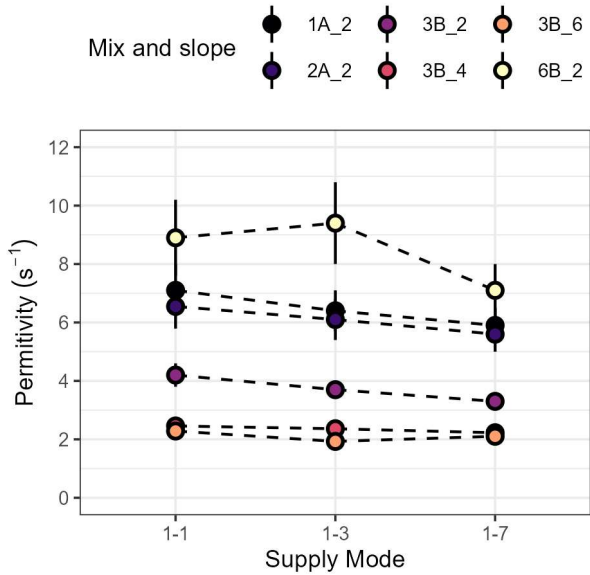
Some minor differences were observed. For example, the permittivity variation with mixture 6B was less than with other mixtures.

The detailed comparison between the different tests focused on the permittivity at maximum discharge, P_{Qmax} , i.e. when all the logs have been supplied whatever the log supply mode (Figure 13:). As for mixture 3B, tests performed with a 2% flume inclination resulted in a permittivity about 50% higher than that measured for other inclinations (3.7 to about 2.2 s^{-1} changing

345

the inclination from 2 to 4-6%). Still for mixture 3B, the permittivity decreased from supply mode 1-1 to supply mode 1-7, with a difference amounting 20% with a flume inclined by 2%. Here again, these effects are attributed to denser packing of

logs with increases of slope or of discharge given to the accumulation to build up. The lowest permittivity at maximum discharge, P_{Qmax} , was obtained with mixture 3B while the highest one was observed with mixture 6B. The ratio between these extreme values was >2 in case of mode supply 1-3. There was no difference between mixtures 1A and 2A, both showing a little decrease trend from supply mode 1-1 to supply mode 1-7. In spite of the large variability for mode supply 1-3, this decrease trend was also observed with mixture 6B.



355 **Figure 13: Permittivity at maximum discharge, P_{Qmax} , for all the tests presented in Table 2 with mixtures 1A, 2A, 3B and 6B and with a flume inclined by 2, 4 and 6%.**

4. Results analysis and discussion

4.1 Insights into the barrier-flow interaction

The presented results allows addressing the interaction between a flexible barrier and a water flow driving woody debris while considering a rather large range of cases. The main aim of this study being to improve barrier design-oriented knowledge, focus is placed on the barrier deformation and loading, while paying a particular attention to the role of the logs accumulation. First, a general description of the flow-barrier interaction is given, based on the general trends derived from the experiments. Differences depending on the mixture characteristics are discussed together with the mechanisms associated. Last, some open questions are raised and discussed.

4.1.1 Main trends concerning the barrier-flow interaction

365 From the first supply, logs were pushed onto the bottom of the barrier, inducing barrier clogging, backwater rise and barrier
bottom loading. The logs accumulated as a plug only, due to small water depth. Any subsequent increase in discharge led to
the obstruction of the newly immersed part of the barrier by logs that were previously accumulated at distance from the barrier,
if any. The distinction between the plug and carpet becomes clearer increasing the discharge and the volume of supplied logs.
The carpet length increased with any further log supply. On the contrary, the carpet length tended to diminish in case no more
370 logs were supplied while increasing discharge.

Both the plug and the carpet contributed to increasing the friction with water, in turn resulting in backwater rise (Risio and
Sammarco, 2020). As previously shown, even a log plug with a limited length may induce a significant backwater rise (Schalko
et al., 2018; Follett et al., 2020). The length of the plug being less than that of the carpet, water preferentially flowed below
the carpet. In case this water flow was sufficiently fast, the drag force applied on some logs in the carpet compensated the
375 buoyancy force and these logs were driven towards the plug, decreasing the carpet length and increasing the plug length (also
see Piton et al, 2023). This phenomenon, by which logs are sucked underwater, was thought to also explain the shorter carpet
observed with higher flume inclinations (Figure 9:). The increase in water flow velocity upstream and under the floating carpet
was also observed to result in a denser log packing at the water surface. This phenomenon was related to higher drag force on
single logs and was supposed to also concern the plug. This was thought to result in a decrease in plug porosity, and
380 consequently in a decrease in permittivity.

The lower permittivity observed for higher flume inclinations (Figure 10:) was attributed to the decrease in plug length and
to the decrease in its porosity, both induced by higher flow velocities. The fact that the permittivity measured with a flume
inclined by 4 or 6% was stable for $Q > 5$ l/s suggested that the plug reached constant hydraulic characteristics whatever the
supply mode. In the case of mode supply 1-7, these constant characteristics were reached before all the logs were supply,
385 suggesting that the logs accumulation permittivity was controlled by part of the total log volume. By contrast, the fact that the
permittivity never stopped decreasing till the higher discharge with a flume inclined by 2% was interpreted as an insufficient
water flow velocity for the logs accumulation to reach constant characteristics (Figure 10: and Appendix B).

Each intercepted log was exposed to a drag force, which was thought to be higher in the plug than in the carpet owing to the
higher local flow velocity resulting from the flow downward diversion below the carpet. By comparison, the drag force on the
390 barrier components was considered much smaller due to the very high barrier porosity and the small diameter of its
components. The drag force applied to each log, from both the plug and carpet, transferred to the flexible barrier through
successive contacts between logs, leading to the barrier deformation. The barrier elongation at mid-height and for the maximum
discharge showed an increase trend with water depth (Figure 14, left). In fact, the lower the logs accumulation permittivity, the
higher the water depth and the higher the drag force on the logs accumulation, resulting in a higher barrier the elongation. In
395 brief, the barrier elongation at mid-height decreased with increasing permittivity, i.e. if water more easily seep through the
accumulation, the accumulation induced a lower load on the barrier (Figure 14, right).

The process of log supply to the river in number and size is stochastic (Comiti et al., 2016). Similarly, rather large variability in system response was observed (Table 2, **Figure 14**). As for the influence of the supply mode, a slight decreasing trend was observed for the permittivity, from mode 1-1 to mode 1-7, for all mixtures and slopes (Figure 13:). This was considered as a secondary effect of the denser accumulations that are more progressively built. Nevertheless, the variation remains very small. As a practical implication, the limited influence of the log supply mode on the permittivity and on the elongation of the barrier indicates that the uncertainty associated with the incoming woody debris rate is not an issue for designers.

4.1.2 Influence of the mixtures characteristics on the system response

No parametric analysis could be conducted from the presented data set as the four woody debris mixtures differed by various parameters (Table 1). Nevertheless, comparing the results obtained with the different mixtures led to clear trends concerning the system response, in terms of barrier elongation, backwater rise and permittivity. These trends complement the description made in the previous section.

Mixtures 1A and 2A had the same volume which was half that of mixtures 3B and 6B. On an other note, the former mixtures resulted in intermediate system responses compared to the two others (**Figure 14**) indicating that the total volume of logs was not a dominating parameter. This observation is to be set against the previous comment concerning the absence of strong correlation between the length of logs accumulated at the surface and the system response (Figure 11: and Figure 12:). It is also in line with the fact the permittivity stopped decreasing before all the logs were supplied in mode 1-7 (Figure 10:). This indicates that only part of the supplied logs controls the system response. It is thought that this response is mainly governed by the log plug, meaning the first portion of logs that accumulate at the barrier but that further supply of logs simply increases the floating carpet length and fill the upstream basin, with marginal effect on the loading and flowing at the barrier.

Mixture 2A consisted in shorter and thinner logs than mixture 1A. Similar length of logs accumulation at the water surface (Figure 11:), water depth and permittivity values (Figure 14:) were obtained with these mixtures, but the barrier elongation was slightly higher with mixture 2A (Figure 14:). This suggests that the dependence of the barrier loading on the backwater rise also accounts for some mechanisms related to load transfer within the logs accumulation, which are thought to depend on some physical characteristics describing the mixture and logs accumulation. In this case, larger loading was associated with shorter logs.

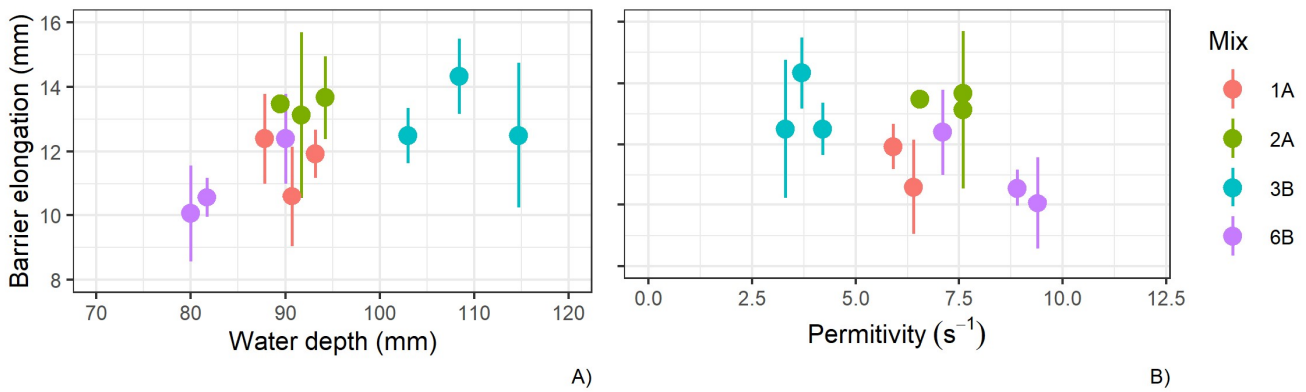


Figure 14: Elongation at barrier mid-height VS water depth (left) and VS permittivity (right) at the end of the tests. Tests with a flume inclined by 2% and considering all supply modes for each mixture

Mixture 3B differed from mixture 6B by longer and thinner logs and a higher number of logs. No significant difference in terms of logs accumulation at the water surface could be observed. Lower barrier elongations and higher permittivity values were obtained with mixture 6B (Figure 13:). The fact that the permittivity values with mixture 6B was more than 60% higher than that of mixture 3B mixture was explained by the lower number of logs and larger log diameter, as the difference in log length could not explain it. Because of this difference in permittivity, a lower water depth was observed with mixture 6B, which is thought to contribute to the lower barrier elongation observed with this mixture. Nevertheless, considering the difference in physical characteristics describing these mixtures, it can't be excluded that some mechanisms involved in load transfer also contributed to this difference in barrier deformation.

Interestingly, while mixtures 2A and 3B resulted in similar barrier mid-height elongations, a much lower backwater rise and, consequently, higher permittivity, was observed with mixture 2A (Figure 13:). Mixture 2A had a volume half that of mixture 3B and consisted in a smaller logs number with smaller diameter and length. Again, this suggests that the dependence of the barrier loading on the backwater rise is very complex, and accounts for various physical characteristics describing the logs. Undoubtedly, the intricacy of this dependence relates to the way the accumulation builds up.

4.2 Some open questions

The system response appeared to depend on many parameters such as the flume inclination and the logs mean length and diameter. By contrast, the influence of the log supply mode and of the total volume of supplied logs was limited or not clearly evidenced. The system response appeared to involve two main mechanisms: barrier clogging and logs accumulation as a plug combined with a floating carpet trapped upstream. The floating carpet was suggested to divert the flow mainly, with limited contribution in the direct load transfer to the barrier. High drag force associated with high local flow velocities was evidenced

to drive logs from the carpet to the plug and to decrease the logs accumulation porosity, globally resulting in a higher barrier loading. A deeper investigation of the system response could focus on the estimation of the cumulated drag force, depending on the log plug porosity and geometrical dimensions. This complex investigation would require measuring the logs accumulation dimensions and porosity, and in particular that of the plug, e.g. with sophisticated techniques as the one used by
450 Follett et al. (2020) on man-made logs accumulations.

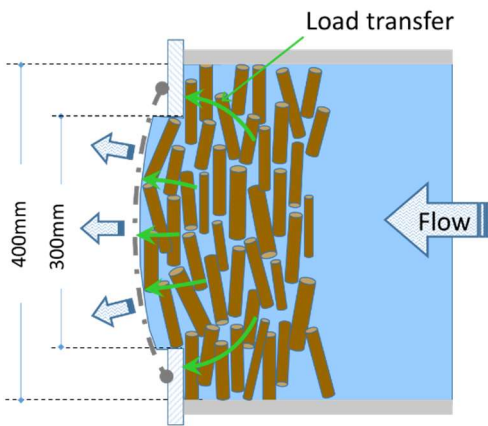


Figure 15: Schematic representation of the logs accumulation at the water surface proposing a load transfer pattern from the logs exposed to drag force to the barrier and lateral Plexiglas walls.

455

The drag force applied to each trapped log transferred to the barrier through contacts between accumulated logs. It was also transferred to the sides of the Plexiglas sheet on which the barrier was secured and reducing the width of the flume at its extremity (Figure 15:). This sheet being rigid while the barrier deforms, arching effects were believed to occur. Arching, which is well known in granular materials, is a phenomenon by which loads are diverted, in this case towards the lateral walls
460 (Chevalier et al., 2007). This load diversion towards the lateral walls attenuates the load on the barrier. This mechanism was thought to be even more pronounced that the ratio between the length of the logs, L_w , and the width of the flexible barrier, b , was pretty high. This is a likely candidate to explain the difference in barrier deformation between mixtures 2A and 1A. These mixtures exhibited very similar values of backwater rise and permittivity but slightly smaller elongations were observed with mixture 1A (with longer and thicker logs). The difference in log length could lead to higher force transfer to the barrier side
465 wings. This could also explain that mixtures 2A and 3B resulted in similar elongation while made from logs with different lengths (Figure 13:). This effect, which contribution is not quantified here, is thought to also occur in the absence of lateral walls, as the river banks also constitute immobile boundaries from which arching will initiate.

4.3 Estimation of the loading exerted on the barrier

The loading on the barrier was estimated from the barrier elongation at mid-height. In a similar manner as in previous research (Song et al., 2017; Hofmann and Berger, 2022), the barrier was assumed to deform as an arc with a length S , a radius R , and a cord length C . In our case, $C= 330$ mm, which is the distance between the barrier cables extremities. The barrier is assumed to be exposed to a uniform pressure, q (Pa), and it is modelled as a continuous elastic body, with a stiffness J (N/m/m).

From the arc length, S , it is possible to compute the arc radius, R , solving the following equation:

$$S = 2 \cdot R \cdot \text{Arcsin}\left(\frac{C}{2 \cdot R}\right) \quad (5)$$

The tensile load in the barrier, T (N), and its deformation, ε (-), being constant along the barrier, it comes that:

$$T = J \cdot \varepsilon = J \cdot \frac{\Delta S}{C} \quad (6)$$

where ΔS is measured during the test and equals $S - C$.

The barrier being exposed to a pressure q , it comes that

$$T = q \cdot R \quad (7)$$

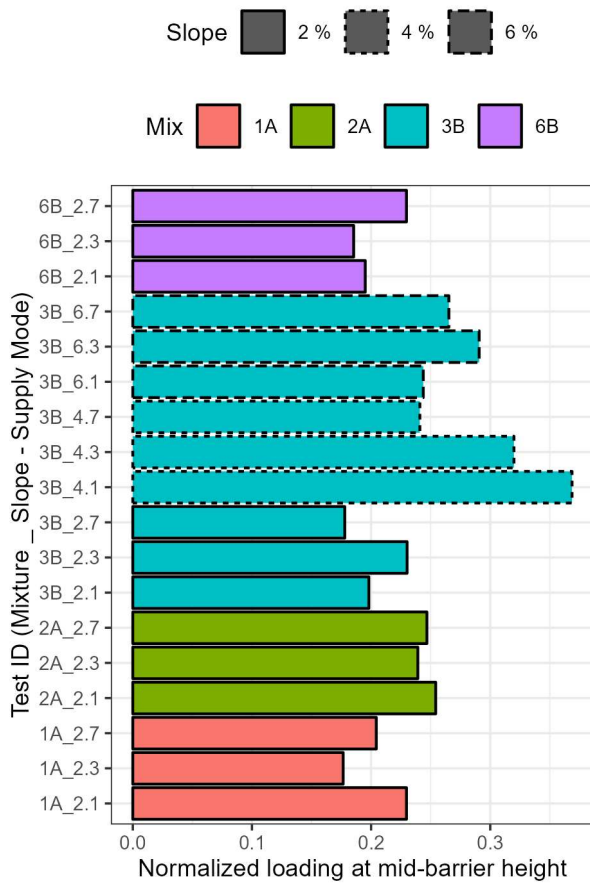
Combining Eq. 6 and 7, q is obtained from:

$$q = \frac{J \cdot \Delta S}{C \cdot R} \quad (8)$$

The stiffness J could not be determined a reliable way from uniaxial tensile tests results. Indeed, these tests revealed that the net stiffness varied with strain, ranging from 30 kN/m/m at low strain to about 6 kN/m/m above a 40 % strain (Lambert et al, 2023). Besides, the loading conditions during uniaxial tensile tests on the net differ to that experienced by the net in the barrier. In the latter case, net necking was restricted due to the top and lower cables resulting in a lower mesh distortion (Lambert et al, 2023). In this context, the value of J was determined from the results of hydrostatic loading tests performed on the barrier. During these tests, the elongation at barrier mid-height reached the value of 40 mm when the water depth was 100 mm, corresponding to a 500 Pa pressure at barrier mid-height. Considering these data, a 23 kN/m/m barrier stiffness was obtained from the previously presented equations. This value is within the range obtained from the tensile tests (30 to 6 kN/m/m) and it is thought to be much more relevant with respect to the loading experienced by the barrier during the flume tests, and particularly at maximum discharge.

The loading experienced by the barrier for the various tests and at maximum discharge was then estimated from the measured elongation at barrier mid-height. This loading was normalized by the hydrostatic pressure at barrier mid-height, which was computed considering the actual water level at maximum discharge in the considered situation (Figure 16:). The ratio covered a wide range, from 17 to 37%. Globally, the highest values were obtained with mixture 3B, with a 4% flume inclination and

not 6% suggesting that the mean water flow velocity was not the only parameter controlling the loading on the barrier. Restricting the analysis to experiments with a 2% flume inclination, the ratio ranged from 17 to 26%.



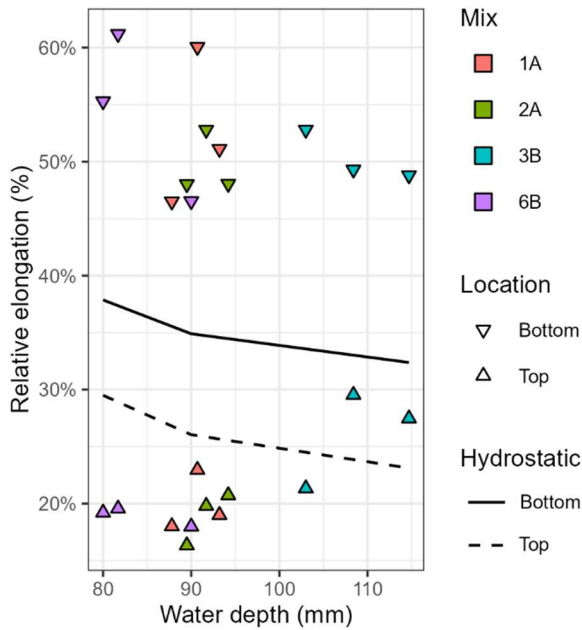
500

Figure 16: Normalized loading at barrier mid-height at maximum discharge. Four mixtures (3B, 1A, 2A and 6B) supplied according to mode 1-1, 1-3 and 1-7.. Plain colour bars stand for 2% flume inclination tests and others stand for 4 and 6% inclinations

505 This finding is of major interest in a design perspective, as it relates the loading experienced by the barrier to hydrostatic loading (Rimböck and Strobl, 2002; Rimböck, 2004; Piton et al 2023). As a first approximation, a linear load distribution from bottom to top, similarly as for hydrostatic loading, may be considered. This assumption was evaluated considering the elongation at the bottom and that at the top of the barrier at maximum discharge during tests with a 2% flume inclination. The elongation values were normalized by the elongation at barrier mid-height under the same situation (Figure 17). The absence of cable at barrier mid-height results in higher elongation values at mid-height than along the top and bottom barrier cables,

510

explaining that relative elongation values are less than one. This figure also shows the normalized elongation at the top and bottom of the barrier computed from the hydrostatic loading test results (HS series on this figure).



515 **Figure 17: Ratio between the barrier elongation measured at the barrier bottom and barrier top to that measured at barrier mid-height at the maximum discharge (tests performed in a flume inclined by 2%). Comparison with the barrier exposed to hydrostatic loading (HS).**

520 HS curves reveal higher relative values at the bottom than at the top. This was due to the higher loading at the barrier bottom than that at the top under hydrostatic loading. This figure thus gives an indication of the load distribution along the vertical axis. Note is made that due to load transfer within the net, elongation of one of the barrier cables should not be interpreted in terms of loading in close proximity of this cable only as it also depends on the barrier loading at distance from the considered cable.

525 Similarly as for HS curves, the relative elongation for tests with woody debris was higher at the bottom than at the top, with average values of about 0.55 and 0.25 respectively. This suggested a much higher loading transferred to the lower cable to that to the top cable. The relative elongation values at the bottom are significantly lower for the HS test, suggesting a higher relative loading at the barrier bottom during the tests with the woody debris. The relative elongation values measured at the top during tests with woody debris are closer to that for the HS test. **Figure 17** also suggested that, by comparison with other mixtures, loading applied on the barrier along the vertical axis was rather uniform with mixture 3B. Indeed, the ratio between the relative

530 elongation at the top and that at the bottom was the highest one with mixture 3B (average of 0.5 vs less than 0.4 for other

mixtures). This was considered to be related to the accumulation of logs above the top of the barrier with mixture 3B, which is associated with water depth higher than 100mm and that resulted in a higher loading on the upper part of the barrier, in particular with respect to that experienced during the HS test. In brief, logs accumulation above the barrier resulted in an additional load on the upper part of the barrier.

535 All these observations are rather consistent with the assumption of a decrease in load from bottom to top of the barrier, with potential additional loading on the barrier upper part when woody debris accumulate above the barrier top cable. In the absence of a more detailed description of the loading exerted by the woody debris on the barrier, it seems acceptable to design the barrier considering a linear load distribution, with a decrease from bottom to top. Reminding that these experiments had similitude with the real-scale, these results suggested that flexible barriers could be designed considering a hydrostatic pressure with a 0.5 reduction factor in case of a channel inclined by 6% maximum and the woody debris consist of large wood only. In case many small wood elements (small branches), leaves or plastic elements are present a higher density of accumulation and a lower permittivity might emerge, possibly resulting in a higher force transfer. This should be confirmed by further investigations.

4.3 Connection with the case of flexible barriers used for debris flows

545 The test method, results and analytical model presented in this research on woody debris may be of interest to the case of debris flows. First, the use of a barrier having mechanical similitude with the real-scale is an innovative approach that could be considered when considering debris flows, as well as the technique for measuring the barrier elongation and the approach for computing the barrier apparent stiffness by comparison with hydrostatic loading (section 4.2). Nevertheless, the results and their interpretation have highlighted some mechanisms revealing differences with possible influence on the barrier loading in particular. The most important difference concerns the fact that a barrier trapping woody debris experiences static loading only. No dynamic loading was evidenced from the barrier elongation measurements under the considered tests conditions, a result consistent with field observation of Rimböck and Strobl (2002). This contrasts with debris flows, for which the impact load is a key design parameter (Wendeler, 2016; Wendeler et al., 2016; Kong et al. 2022, 2023). On a phenomenological view point, the intercepted logs form a rather permeable accumulation, which is slowly building up and with many logs close to the surface. This significantly differs with debris flows, for which the trapped solid material tend to more suddenly pile-up against the barrier, forms a dead zone starting from the barrier bottom and which is much less permeable. In addition, with large wood, the barrier upper part is exposed to a significant additional load due to logs accumulating above the barrier upper cable, held in place by other protruding logs (Figure 2). This is believed to result in a different load distribution along the vertical axis as compared to the case of debris flow barriers, even if overflowed (Wendeler, 2016; Berger et al., 2021).

555

560 Finally, the loading exerted by the flow on the barrier was evaluated to be less than 0.5 times the hydrostatic loading. By contrast, the design of flexible barriers exposed to debris flows accounts for a static load at least 1.6 times the hydrostatic load

combined with a dynamic load (Wendeler, 2016; Berger et al., 2021). The loading applied on the barrier resulting from trapped woody debris is thus much less than that due to debris flows.

Conclusion

565 This article has investigated the interaction between a flexible barrier and woody-debris laden flows, in view of improving the design of these barriers to resist the induced loading. Small-scale experiments were conducted considering different woody debris mixtures, supply modes and flume inclinations. These experiments had similitude with the real-scale, including for what concerns the barrier, allowing for the extrapolation of the findings to real structures and their design. A model was proposed for deriving the static loading applied on the barrier from its elongation at maximum discharge. This model was based on the following assumptions: (1) the barrier deforms as an arch, (2) it is exposed to a uniform loading, normal to the barrier, (3) the barrier is a continuous and elastic body, and (4) the problem is treated in 2D, assuming no influence of the barrier loading on its upper and lower parts. In an original manner, the barrier stiffness was derived from tests where the barrier was exposed to an hydro-static loading.

The main findings from this study were the following:

- 575
1. The loading on the barrier is significantly influenced by the water flow mean velocity, strongly driven by flow discharge and torrent bed inclination, as well as the woody debris characteristics (diameter and length).
 2. The barrier loading is inversely proportional to the capacity of the woody debris accumulation to let the water seep through, which can be expressed in terms of permittivity. This latter is controlled by the logs accumulation porosity and log diameter in particular.
 - 580 3. The permittivity of the system appeared to depend on the way the accumulation builds up and on the evolution of its characteristics with increasing discharge and volume of logs trapped.
 4. The logs accumulation permittivity was determined to range from 2 to 10 s⁻¹, corresponding to a 0.32-1.6 s⁻¹ range at the real-scale.
 5. Logs may accumulate above the barrier top cable without passing over the barrier. In the test conditions of this study, the additional load on the upper part of the barrier induced by this accumulation resulted in a moderate top cable additional elongation.
 - 585 6. Considering a loading equivalent to hydrostatic loading for designing flexible barriers aimed at trapping woody debris is conservative. The presented results suggested considering a reduction factor of 0.5.

Symbols

590 h : water depth upstream the barrier (m)

h_0 : water depth upstream the barrier with a pure water flow (m)

h^* : increase in water depth upstream the barrier due to the accumulation of woody debris (m)

Q : discharge ($\text{l}\cdot\text{s}^{-1}$)

μ : weir coefficient (-)

595 b : width of the rectangular opening in the Plexiglas sheet (m)

g : gravity acceleration ($\text{m}\cdot\text{s}^{-2}$)

Fr_0 : Froude number (-)

P : permittivity of the logs accumulation (s^{-1})

P_{Qmax} : permittivity of the logs accumulation at maximum discharge (s^{-1})

600 **Data Availability Statement**

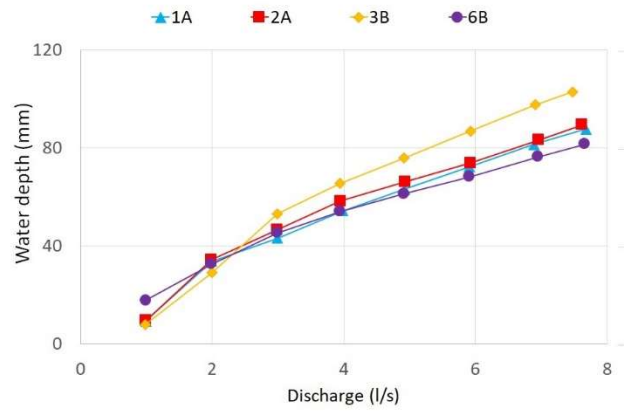
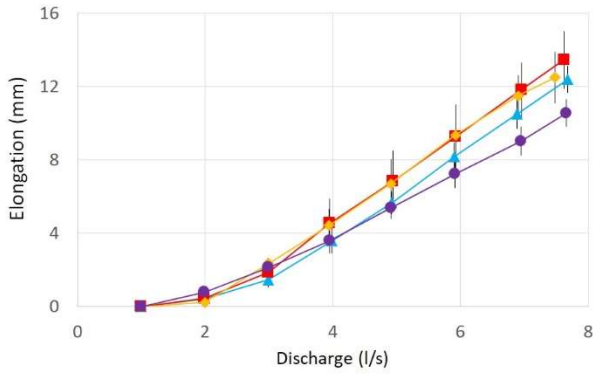
All data generated or used during the study are available in a repository online in accordance with funder data retention policies: FilTor: Interaction between flexible barriers and flows (INRAE), <https://data.inrae.fr/dataverse/filtor>, backwater rise and LW releases: <https://doi.org/10.15454/RMIEJM>, and flexible barrier elongation measurement: <https://doi.org/10.15454/9HUDGG>.

Acknowledgements

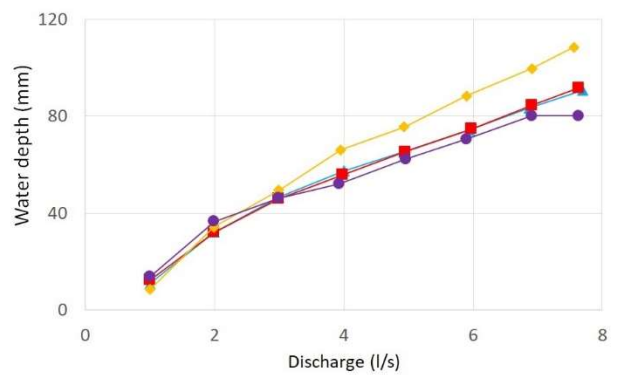
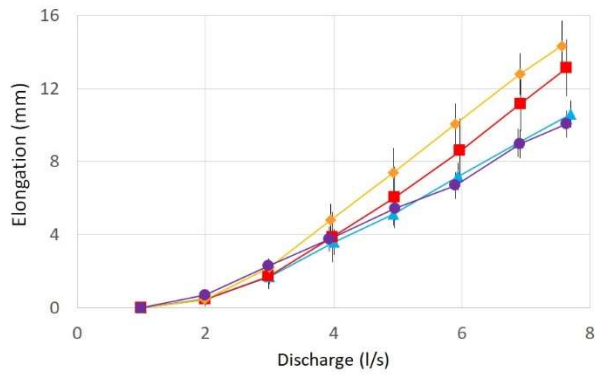
605 The authors would like to thank Ana-Rocio CERON-MAYO who performed the experiments and contributed to the previous analysis, Hervé BELLOT and Alexis BUFFET for their help in designing the experimental set up and two anonymous reviewers for providing helpful comments on a previous version of this paper This work was funded by the French Ministry of Environment (Direction Générale de la Prévention des Risques—Ministère de la Transition Ecologique et Solidaire) within the multirisk Agreement SRNH-IRSTEA 2019 (Action FILTOR).

610

Mode supply 1-1



Mode supply 1-3



Mode supply 1-7

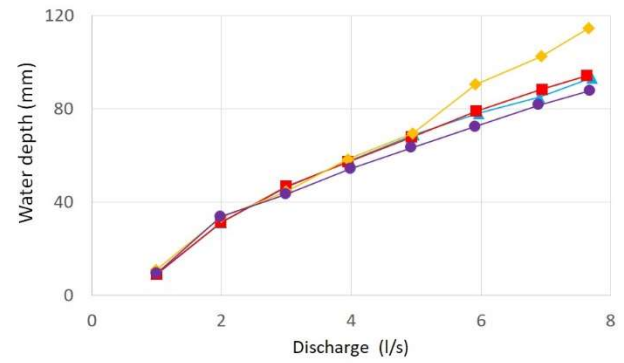
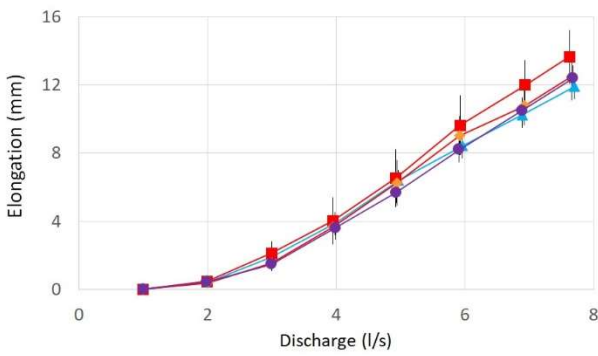


Figure A1: Elongation at barrier-mid-height and water depth with increasing discharge, for all mixtures during tests with a 2% flume inclination.

Appendix B

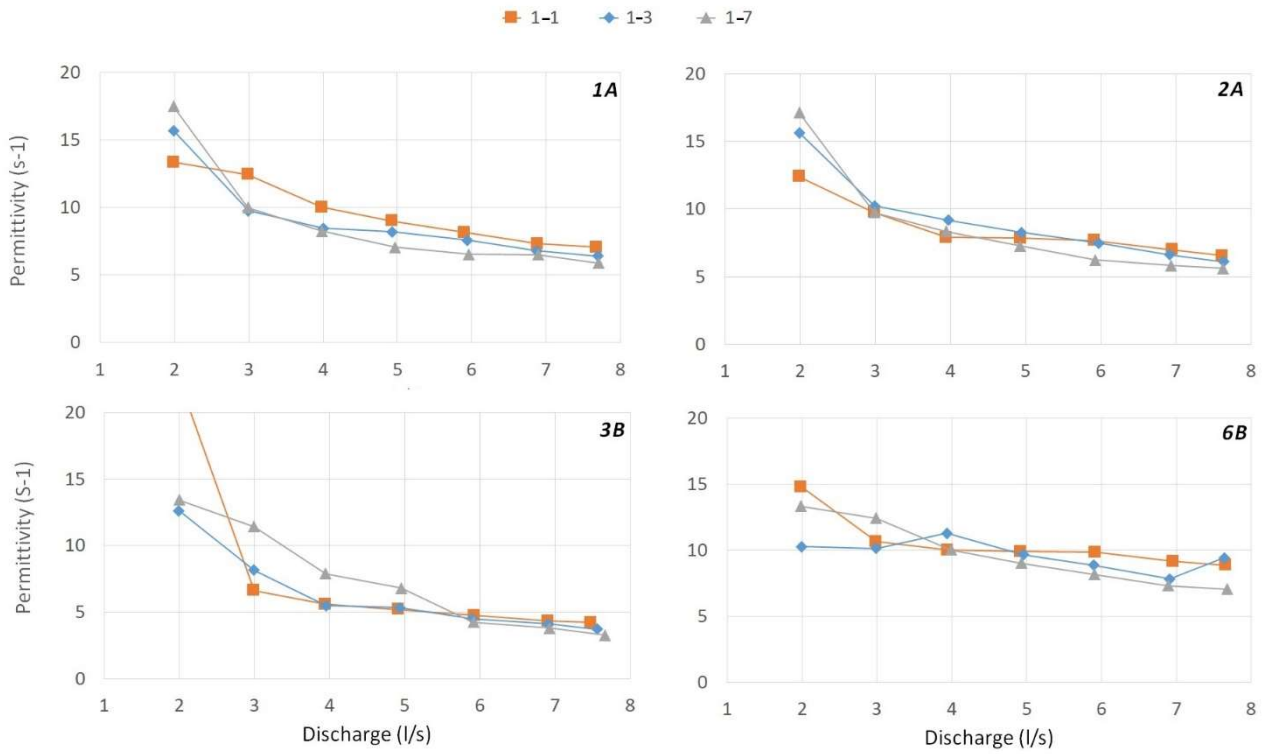


Figure B1: Permittivity at maximum discharge, P_{Qmax} , with increasing discharge for all tests at a 2% flume inclination.

625

630

References

- Albaba, A, Lambert, S., Kneib, F., Chareyre, B., and Nicot, F.: DEM Modeling of a flexible barrier impacted by a dry granular flow, *Rock Mech. Rock Eng.*, 50, 3029–3048, doi:10.1007/s00603-017-1286-z, 2017.
- Berger, C. and Denk, M. and Graf, C. and Stieglitz, L. and C. Wendeler. Practical guide for debris flow and hillslope debris flow protection nets. *WSL Berichte*, 113, 267, 2021.
- Chevalier, B., Combe, G., and Villard, P.: Load transfers and arching effects in granular soil layer, in: *Proceedings of the 18th Congrès Français de Mécanique*, Grenoble, France, 27-31 August 2007, 6 p., 2007.
- Choi, C.E., and Goodwin, G.R.: Interaction between granular flows and flexible obstacles: a grain-scale investigation, *Comput. Geotech.*, 128, doi:10.1016/j.compgeo.2020.103800, 2020.
- De Cicco PN, Paris E, Solari L, Ruiz-Villanueva V. Bridge pier shape influence on wood accumulation: Outcomes from flume experiments and numerical modelling. *J Flood Risk Management*. 2020;13:e12599. <https://doi.org/10.1111/jfr3.12599>
- Comiti, F., Lucía, A., and Rickenmann, D.: Large wood recruitment and transport during large floods: A review. *Geomorphology*, 269, 23–39, doi:10.1016/j.geomorph.2016.06.016., 2016.
- Faure, Y., Farkouh, B., Delmas, P. and Nancey, A.: Analysis of geotextile filter behaviour after 21 years in Valcros dam. *Geotext. Geomembr.*, 17, 353–370, doi:10.1016/S0266-1144(99)00010-2, 1999.
- Follett, E., Schalko, I., & Nepf, H.(2020). Momentum and energy predict the backwater rise generated by a largewood jam. *Geophysical Research Letters*, 47, e2020GL089346. <https://doi.org/10.1029/2020GL089346>
- Gasser, E., Schwarz, M., Simon, A., Perona, P., Phillips, C., Hübl, J., and Dorren, L.: A review of modeling the effects of vegetation on large wood recruitment processes in mountain catchments, *Earth Sci. Rev.*, 194, 350–373, doi:10.1016/j.earscirev.2019.04.013, 2019.

Hofmann, R.; Berger, S. Impacts of Gravitational Mass Movements on Protective Structures—Rock Avalanches/Granular Flow. *Geosciences*, Doi:10.3390/geosciences12060223, 2022.

665

ICOLD. Blockage of Reservoir Spillways, Intakes and Bottom Outlets by Floating Debris, International Commission On Large Dams, <https://www.icoldchile.cl/boletines/176.pdf> , accessed 2023-05-22, 2019.

670 Kong, Y., Guan, M., Li, X., Zhao, J., & Yan, H.: Bi-linear laws govern the impacts of debris flows, debris avalanches, and rock avalanches on flexible barrier. *Journal of Geophysical Research: Earth Surface*, 127, e2022JF006870. <https://doi.org/10.1029/2022JF006870>, 2022.

Kong, Y. and Li, X. and Zhao, J. and Guan, M. : [Load-deflection of flexible ring-net barrier in resisting debris flows](https://doi.org/10.1680/jgeot.22.00135), *Géotechnique* <https://doi.org/10.1680/jgeot.22.00135>, 2023

675

Lambert, S., Bourrier, F., Ceron-Mayo, A-R, Dugelas, L., Dubois, F., and Piton, G.: Small-Scale Modeling of Flexible Barriers. I: Mechanical Similitude of the Structure, *J. Hydraul. Eng.*, 149, doi:10.1061/JHEND8.HYENG-13070, 2022.

680 Lange, D., and Bezzola, G.: Schwemmholz - Probleme und Lösungsansätze [Driftwood - Problems and solutions], <https://ethz.ch/content/dam/ethz/special-interest/baug/vaw/vaw-dam/documents/das-institut/mitteilungen/2000-2009/188.pdf>, accessed 2023-05-22, 2006.

685 Lucia, A., Comiti, F., Borga, M., Cavalli, M. and Marchi, L.: Dynamics of large wood during a flash flood in two mountain catchments. *Nat. Hazards Earth Syst. Sci.*, 15, 1741-1755, doi:10.5194/nhess-15-1741-2015, 2015.

Ng, C.W.W., Song, D., Choi, C.E., Liu, L.H.D., Kwan, J.S.H., Koo, R.C.H., and Pun, W.K.: Impact mechanisms of granular and viscous flows on rigid and flexible barriers, *Can. Geotech. J.*, 54, 188–206, doi:10.1139/cgj-2016-0128, 2017.

690

Okamoto T, Takebayashi H, Sanjou M, Suzuki R, Toda K. Log jam formation at bridges and the effect on floodplain flow: A flume experiment. *J Flood Risk Management*. 2020;13(Suppl.1):e12562. <https://doi.org/10.1111/jfr3.12562>

- 695 Piton, G., Ceron Mayo, A.R., and Lambert, S.: Small-Scale Modeling of Flexible Barriers. II: Interactions with Large Wood, *J. Hydraul. Eng.*, 149, doi:10.1061/JHEND8.HYENG-13071, 2022.
- Piton, G., Horiguchi, T., Marchal, L., and Lambert, S.: Open check dams and large wood: head losses and release conditions, *Nat. Hazards Earth Syst. Sci.*, 20, 3293–3314, doi:10.5194/nhess-20-3293-2020, 2020.
- 700 Piton, G., and Recking, A.: Design of sediment traps with open check dams. II: woody debris. *J. Hydraul. Eng.*, 142, 1–17, doi:10.1061/(ASCE)HY.1943-7900.0001049, 2015.
- Piton, G., and Recking, A.: Steep Bedload-Laden Flows: Near Critical?, *J. Geophys. Res. Earth. Surf.*, 124, 2160–2175, doi:10.1029/2019JF005021, 2019.
- 705 Rimböck, A.: Design of rope net barriers for woody debris entrapment: introduction of a design concept, in: proceedings of 10th Interpraevent Symposium, Riva del Garda, Italy, 265–276, http://www.interpraevent.at/palm-cms/upload_files/Publikationen/Tagungsbeitraege/2004_3_VII-265.pdf, accessed 2023-05-22, 2004.
- 710 Rimböck, A., and Strobl, T.: Loads on rope net constructions for woody debris entrapment in torrents, in: proceedings of Interpraevent Symposium, Matsumoto, Japan, 14-18 October 2002, 797–807, http://www.interpraevent.at/palm-cms/upload_files/Publikationen/Tagungsbeitraege/2002_2_797.pdf, accessed 2023-05-22, 2002
- 715 Di Risio, M., and Sammarco P.: Effects of floaters on the free surface profiles of river flows, *Environ. Fluid Mech.*, 20, 527–537, doi:10.1007/s10652-019-09710-z, 2020.
- Ruiz-Villanueva V., Mazzorana, B., Bladé, E., Burkli, L., Iribarren-Anacona, P., Mao, L., Nakamura, F., Ravazzolo, D., Rickenmann, D., Sanz-Ramoz, M., Stoffel, M. and Wohl, E.: Characterization of wood-laden flows in rivers, *Earth Surf. Process Landf.*, 44, 1694–1709, doi:10.1002/esp.4603, 2019.
- 720 Ruiz-Villanueva, V., Bodoque, J.M., Díez-Herrero, A., and Bladé E.: Large wood transport as significant influence on flood risk in a mountain village, *Nat. Hazards*, 74, 967–987, doi:10.1007/s11069-014-1222-4, 2014.

- 725 Schalko, I., Schmocker, L., Weitbrecht, V., and Boes, R.M., Backwater rise due to large wood accumulations, *J. Hydraul. Eng.*, 144, 9 doi:10.1061/(ASCE)HY.1943-7900.0001501, 2018.
- Schalko, I., Lageder, C., Schmocker, L., Weitbrecht, V., and Boes, R.M.: Laboratory flume experiments on the formation of spanwise large wood accumulation Part I: Effect on backwater rise, *Water Resour. Res.*, 55, 4854–
730 4870, doi:10.1029/2018wr024649, 2019.
- Schalko, I., Lageder, C., Schmocker, L., Weitbrecht, V., Boes, R.M.: Laboratory flume experiments on the formation of spanwise large wood accumulations Part II: Effect on local scour, *Water Resour. Res.*, 55, 4871–
4885. doi:10.1029/2019WR024789, 2019.
- 735
- Schmocker, L., and Hager, W.H.: Scale modeling of wooden debris accumulation at a debris rack, *J. Hydraul. Eng.*, 139, 827–836. doi:10.1061/(ASCE)HY.1943-7900.0000714, 2013.
- Schmocker, L., and Weitbrecht, V.: Driftwood: Risk analysis and engineering measures, *J. Hydraul. Eng.*, 139,
740 683–695, doi:10.1061/(ASCE)HY.1943-7900.0000728, 2013.
- Song, D. and Choi, C. E. and Ng, C. W. W. and Zhou, G. G. D. : Geophysical flows impacting a flexible barrier: effects of solid-fluid interaction, *Landslides*, doi:10.1007/s10346-017-0856-1, 2017.
- 745 Wendeler, C., 2016: Debris-flow protection systems for mountain torrents. Basic principles for planning and calculation of flexible barriers. *WSL Berichte*, 44. Birmensdorf, Swiss Federal Institute for Forest, Snow and Landscape Research WSL. 267 p.
- Wendeler, C., and Volkwein, A.: Laboratory tests for the optimization of mesh size for flexible debris-flow
750 barriers, *Nat. Hazards Earth Syst. Sci.*, 15, 2597–2604, doi:10.5194/nhess-15-2597-2015, 2015.
- Wendeler, C., Volkwein, A., McArdeall B.W., and Bartelt, P.: Load model for designing flexible steel barriers for debris flow mitigation, *Can. Geotech. J.*, 56, 893–910, doi:10.1139/cgj-2016-0157, 2019.